universe

IMPACT FACTOR 2.9

CITESCORE 3.6

Article

Axionic Dark Matter in a Bi-Metric Universe

Carlos Maldonado and Fernando Méndez

MDPI

https://doi.org/10.3390/universe9100429

universe

MDPI

Article

Axionic Dark Matter in a Bi-Metric Universe

Carlos Maldonado * and Fernando Méndez

Departamento de Física, Facultad de Ciencia, Universidad de Santiago de Chile (USACH), Santiago 9170124, Chile; fernando.mendez@usach.cl
* Correspondence: carlos.maldonados@usach.cl

Abstract: We study the evolution and production of axion dark matter in a universe model with two scale factors corresponding to different patches of the universe. The interaction between patches is described through a deformed Poisson bracket structure. The first part of the present paper is devoted to a review of the results reported in previous works concerning the study of dark matter as WIMPs and FIMPs. The new results concerning axionic dark matter in this bi-metric scenario show that different values of the deformation parameter κ allow values of masses and misalignment angles forbidden in standard cosmology. The present model can also be considered a different type of nonstandard cosmology consistent with previously reported results.

Keywords: non-standard cosmology; dark matter; quantum gravity phenomenology

Citation: Maldonado, C.; Méndez, F. Axionic Dark Matter in a Bi-Metric Universe. *Universe* **2023**, *9*, 429. https://doi.org/10.3390/universe9100429

Academic Editor: Antonino Del Popolo

Received: 17 July 2023
Revised: 15 September 2023
Accepted: 20 September 2023
Published: 27 September 2023

1. Introduction

The quest for a concise description of the four fundamental interactions, or the intriguing fact that only three of them admit a unified description based on quantum principles as well as Lorentz invariance, encourages the efforts in the search of a quantum theory of gravity (QG) [1–5].

Quantum gravity phenomenology, on the other hand, has attracted much attention in recent years [6–10]. Indeed, the possibility that the structure of spacetime, at the Planck scale, might not be a continuous, four- dimensional Minkowski manifold can be understood as a relic of some underlying QG theory, as this happens in proposals like Lorentz invariance violation, noncommutative geometry or low-energy limits of loop quantum gravity [11–14].

In the same spirit, a different proposal is the so-called noncommutative fields, where the fields themselves satisfy a deformed commutation relation [15–17]. In this approach, spacetime maintains its structure, and the fields capture possible signals of the QG through the deformed commutation relations.

This arena is suitable for analyzing the problem of gravity, where spacetime itself is the object of interest. On the other hand, since any effect of the QG would (should) be suppressed at scales far from Planck's scale, it seems reasonable to look for relics of this noncommutativity at cosmological scales.

The noncommutative Landau problem inspired the model under consideration in quantum mechanics [18,19], even though we discuss the idea at the classical level. The concrete realization of the model has been developed in a series of papers [20–24], where a cosmology with two scale factors has been introduced together with a deformed Poisson algebra structure, implying nontrivial interactions [25–28].

Let us review the main features of the proposal. The metric satisfying the cosmological principle of homogeneity and isotropy is the Friedmann–Lemaitre–Robertson–Walker (FLRW) metric, namely

$$ds^2 = dt^2 + a^2(t)\left(\frac{dr^2}{1-kr^2} + r^2\, d\Omega^2\right). \tag{1}$$

Here, $a(t)$ is the scale factor, r is the radial (dimensionless) coordinate, and k is the curvature of the spatial sections.

The Einstein equations for this metric (in the absence of matter) can be derived from the following Hamiltonian:

$$H = \frac{NG}{2}\left[\frac{\pi_a^2}{a} + \frac{1}{G^2}\left(a\,k - \frac{\Lambda}{3}a^3\right)\right], \tag{2}$$

where π_a is the conjugate momenta of a (the canonical dimension of the scale factors is +1) and N is an auxiliary field (chosen to be $N = 1$ at the end of calculations) related to the time invariance reparametrization. The spatial curvature is k, and Λ is the cosmological constant. The Poisson bracket structure is standard. Namely, the only non-vanishing bracket is $\{a, \pi\} = 1$.

The model proposed in [20] considers two scale factors, namely $a(t)$ and $b(t)$, describing (possibly) two sectors of the universe. The interpretation of the two scale factors is an open issue. Indeed, it might describe two patches causally disconnected, or it might describe two universes. We adopt the term 'patch' to refer to a particular sector (patch a or patch b).

Then, the model is described by a Hamiltonian

$$H = H_a + H_b, \tag{3}$$

with H_a given by Equation (2), while H_b has the same form as H_a but for the scale factor b with canonical conjugate momenta π_b. The spatial curvature and cosmological constant can also be chosen differently for each patch (k_a, k_b and Λ_a, Λ_b, respectively). In principle, it is also possible to choose different N values for the two patches, but the time coordinate is the same for the whole system.

The field equations are obtained from the previous Hamiltonian and the Poisson bracket structure of the theory. If Poisson brackets are canonical for the sets (a, π_a) and (b, π_b) while they are zero between the scale factors and momenta belonging to different patches, then the model describes two independent copies of an FLRW universe. But if nontrivial Poisson brackets occur between scale factors or momenta from different patches, then the two patches evolve with an interacting term connecting both dynamics.

The situation is similar to the following. Consider the Hamiltonian $H = \frac{1}{2}\pi^i\pi_i$ (with an index $i \in \{1, 3\}$) in a phase space with the coordinates (x^i, π_j). For a canonical Poisson bracket structure, the previous Hamiltonian describes just a free particle. However, for the particular choice $\{\pi_i, \pi_j\} = e\,\epsilon_{ijk}B^k$, the system corresponds to a particle with a charge e interacting with a magnetic field B^k. Indeed, the equation of motion for this system is $\ddot{\mathbf{x}} = e\,\dot{\mathbf{x}} \times \mathbf{B}$.

In the present case, the Poison bracket structure that introduces the interaction between the patches is

$$\{a_\alpha, a_\beta\} = 0, \quad \{a_\alpha, \pi_\beta\} = \delta_{\alpha\beta}, \quad \{\pi_\alpha, \pi_\beta\} = \theta\,\epsilon_{\alpha\beta}, \tag{4}$$

with θ as a constant parameter. The index α denotes patches a or b, and the same holds for index β. Then, the deformation is introduced through the momenta of the fields, namely $\{\pi_a, \pi_b\} = \theta$, while the other possible deformations (such as $\{a, b\}$) are zero. On the other hand, the Poisson bracket structure for each patch remains canonical. We will use the dimensionless parameter $\kappa = \theta\,G$ as the deformation parameter.

First-order field equations can be recast as second-order ones as follows:

$$2a\ddot{a} + \dot{a}^2 = \Lambda_a\,a^2 - k_a + 2\kappa\dot{b}, \tag{5}$$

$$2b\ddot{b} + \dot{b}^2 = \Lambda_b\,b^2 - k_b - 2\kappa\dot{a}, \tag{6}$$

along with the first-order constraint

$$a\dot{a}^2 + b\dot{b}^2 = \frac{\Lambda_a}{3}\, a^3 - k_a\, a + \frac{\Lambda_b}{3}\, b^3 - k_b\, b. \tag{7}$$

The model describes a Λ-dominated era. The solutions exhibit oscillatory or inflationary behavior, depending on the values of the parameter κ. The periods with accelerated or decelerated expansion are also periodic. The model exhibits a dynamical dark energy content, even for the vanishing cosmological constant [20].

Different Poisson bracket deformations have been analyzed in this context. For example, in [21], it was shown that it is possible to map a mechanical system of two particles in the presence of a constant magnetic field to a model of cosmology with two scale factors [22]. The case in which the Poisson bracket between the two scale factors is not zero, as well as the momentum, was analyzed in [22], suggesting a possible connection of the model with the problem to primordial magnetic fields [29,30].

Deformed Poisson bracket structures as a source of interactions have also been investigated in different contexts, mostly in the case of noncommutative quantum mechanics [18,31–33] and recently in the proposal of the so-called metaparticles [34] as well as its implication for cosmology [35–38].

It is natural to ask now what happened to matter's evolution in this scenario. This problem was investigated in [23] and applied to the case of dark matter (DM) modeled as WIMPs and FIMPs. Section 2 is devoted to a review of the results obtained in [23,24]. Section 3 is devoted to analyzing axionic DM in the two-scale factor model. In Section 4, we present a discussion of the results and the conclusions.

2. A Review on Barotropic Matter and Dark Matter in the Two-Scale Factor Universe

Before discussing the axionic dark matter (DM) in the model of the universe with two metrics, we will briefly review the results in [23,24] concerning the problem of the evolution of ordinary matter and DM in the model. The WIMP and FIMP production mechanisms were studied for the DM, in contrast with the present work, where DM as axionic matter is considered.

The inclusion of barotropic matter in the two patches was addressed in [23] under the following assumptions: (1) the matter content of one patch does not interact with the matter content of the second patch, and (2) the matter on each patch is described as a barotropic fluid.

These assumptions translate into the following evolution equations for the scale factors and matter density in the matter-dominated era (thus $\Lambda_a = 0 = \Lambda_b$) and for a flat three-dimensional space [39] ($k_a = 0 = k_b$):

$$H_a^2 = \frac{\rho_a}{3}, \tag{8}$$

$$H_b^2 = \frac{\rho_b}{3}, \tag{9}$$

$$\dot{\rho}_a + 3H_a(\omega_a + 1)\rho_a = \Gamma_a\, \rho_a, \tag{10}$$

$$\dot{\rho}_b + 3H_b(\omega_b + 1)\rho_b = -\Gamma_b\, \rho_b, \tag{11}$$

with

$$\Gamma_a = 2\kappa \frac{b}{a^2}\, \delta^{1/2}, \quad \Gamma_b = 2\kappa \frac{a}{b^2}\, \delta^{-1/2}, \tag{12}$$

where $\delta = \rho_b/\rho_a$. The decay functions Γ satisfy $a^3\Gamma_a - b^3\Gamma_b = 0$. Here, H is the Hubble parameter defined on each patch. The energy density ρ and pressure p are related by the barotropic fluid condition $p = \omega\, \rho$ with, in principle, a different barotropic index for each patch.

It is worth noticing that Equations (10) and (11) define a sort of nonstandard cosmology (NSC) [40–45]. But the role of the extra field—characteristic of the usual NSC where a scalar field is introduced to modify the universe's expansion rate—is played here by the matter in

the other patch. On the other hand, the decay rate depends on the energy density in both patches, and the geometry through the scale factors and is no longer a constant.

A consequence of this evolution is the *source-sink* effect of the energy density; that is, energy from one patch drains to another, modifying the energy content there. In Figure 1, the numerical solution for relativistic matter in a ($\omega_a = 1/3$) and nonrelativistic matter in b ($\omega_b = 0$) with a symmetric initial condition ($\rho_a(0) = \rho_b(0)$) is shown as a function of the ratio T/T_0, with T_0 being the present temperature of the universe.

In the figure, the field in b is no longer effective (all the energy has been drained already) at $T_{\rm end}/T_0$. The vertical line $T_{\rm BBN}/T_0$ denotes the temperature of Big Bang nucleosynthesis (BBN). In the case depicted here, the process ends before the BBN epoch ($T_{\rm BBN} \simeq 4$ GeV), and therefore, the drainning process is *safe* in the sense that it does not conflict with astrophysical data [46,47], and the standard cosmology is recovered for temperatures lower than $T_{\rm BBN}$. Note, finally, that for a given δ, the temperature of the total drain depends only on κ.

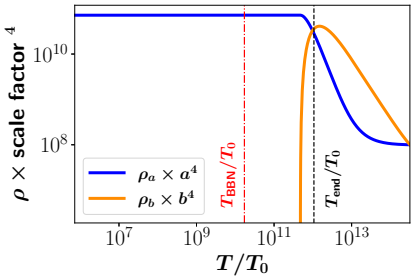

Figure 1. Energy densities for $\omega = 0$, $\kappa = 10^{-35}$, and $\delta = 1$. The dashed line represents the temperature at which the field on patch b is no longer effective ($T_{\rm end}$).

This result posits a natural question: What happens in the case of dark matter? In [24], this question was addressed in the WIMPs and FIMPs DM scenario. Let us review the results obtained there.

If the number density of DM $n_{\rm DM}$ is assumed to obey the Boltzmann equation, and it is present in the a-patch, then

$$\frac{dn_{\rm DM}}{dt} + 3H_a\, n_{\rm DM} = -\langle\sigma v\rangle \left(n_{\rm DM}^2 - n_{\rm eq}^2\right), \tag{13}$$

where $\langle\sigma v\rangle$ is the thermal average annihilation cross-section and $n_{\rm eq}$ is the equilibrium number density for DM.

To investigate the evolution of dark matter, it is assumed that the relic density is established in a radiation era in the standard cosmological model and, in this case, will be considered similarly. (DM will be only on the patch a.) The models of weak interacting massive particles (WIMPs) and feebly interacting massive particles (FIMPs) were discussed in [24]. Both models consist of massive particles, with the production mechanism being the main difference. The so-called WIMPs [48–51] are thermally produced via the freeze out (FO) mechanism [52], while FIMPs [53–55] are generated in a nonthermal mechanism like the freeze in (FI) mechanism [56–58].

The energy density evolution equations for the bi-metric universe are given by the following (see Equations (10) and (11)):

$$\dot{\rho_a} + 4\frac{\dot{a}}{a}\rho_a = 6\kappa M_{\rm Pl}^3 \frac{\dot{a}\dot{b}}{a^3}, \tag{14}$$

$$\dot{\rho_b} + 3(\omega+1)\frac{\dot{b}}{b}\rho_b = -6\kappa M_{\rm Pl}^3 \frac{\dot{a}\dot{b}}{b^3}, \tag{15}$$

while the time evolution of the scale factors, considering that in our model, the DM is only in the patch a, is

$$\dot{a} = a\sqrt{\frac{\rho_a + \rho_{\rm DM}}{3M_{\rm Pl}^2}}, \tag{16}$$

$$\dot{b} = b\sqrt{\frac{\rho_b}{3M_{\rm Pl}^2}}. \tag{17}$$

The DM content is described by Equation (13) for the case of WIMPs and FIMPs.

To summarize, the set of Equations (13)–(17) allows one to obtain the DM density and barotropic matter density evolution in the patch a for a given matter content (barotropic) in patch b.

In the case of WIMPs (produced through the FO mechanism), the DM particles are in thermal equilibrium with all the particles in the bath in the early universe. Their interactions become inefficient to keep them in the bath as long as the universe expands. Therefore, they leave the thermal bath and freeze their number.

These kinds of particles are very popular due to, among other properties, the so-called WIMP miracle; that is, for $\langle\sigma v\rangle$ of the order of the electro-weak interactions (i.e., $\langle\sigma v\rangle \approx 10^{-9}$ GeV $^{-2}$), the DM relic density at present agrees with the current measurements.

FIMPs, on the other hand, are produced out of the thermal bath (FI mechanism). Therefore, they never reach equilibrium, and their interactions are feeble, causing their number to freeze.

For WIMPs the analytic solution of Equation (13) is obtained in the limit $n_{\rm DM} \gg n_{\rm eq}$, while for FIMPs, the appropriate limit is $n_{\rm DM} \ll n_{\rm eq}$. The parameter of interest is the DM yield (Y), defined as $Y \equiv n_{\rm DM}/s$, with s as the entropy density of the universe. It can be estimated as follows:

$$Y_{\rm WIMPS} \propto \frac{1}{M_{\rm DM} J(x_{\rm fo})}, \quad Y_{\rm FIMPS} \propto M_{\rm DM}\langle\sigma v\rangle. \tag{18}$$

with $M_{\rm DM}$ as the DM mass particle. Here, J is a function of the temperature through the dimensionless parameter $x = M_{\rm DM}/T$, namely $J(x_{\rm fo}) = \int_{x_{\rm fo}}^{\infty} x^{-2}\langle\sigma v\rangle(x)dx$. The integration starts at $x_{\rm fo}$ when the DM particle freezes its number. Note that if the thermal average cross-section is constant, then the integral turns out to be $\langle\sigma v\rangle/x_{\rm fo}$.

In contrast, the yield for FIMPs is directly proportional to the thermal average annihilation cross-section.

The effect of considering a universe with two scale factors with an interaction induced through the Poisson bracket deformation is a drain of energy from one patch to the other, as DM is for extending the range of DM parameters allowed. We reproduced some of the numerical results obtained in [24] to see this.

Figure 2 shows the yield of DM in terms of x for $M_{\rm DM} = 100$ GeV and $\langle\sigma v\rangle = 10^{-11}$ GeV^{-2}. The dashed line ($x_{\rm fo}$) shows the temperature at which DM decouples from the thermal bath and starts to freeze their number. The BBN temperature ($x_{\rm BBN}$), on the other hand, is marked with a dot-dashed line. Finally, the green horizontal strip represents the current relic density of DM. The parameters $M_{\rm DM}$ and $\langle\sigma v\rangle$ used in this figure are excluded in the ΛCDM model because they overproduce the current DM relic density.

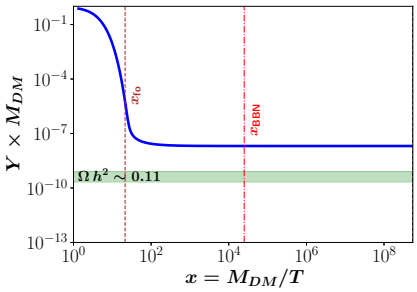

Figure 2. The yield of dark matter particles in standard cosmology. For the DM mass $M_{\rm DM} = 100$ GeV and thermal average annihilation cross-section $\langle \sigma v \rangle = 10^{-11}$ GeV^{-2} established in the freeze out mechanism, overproduction of DM at present was observed.

The evolution of the yield for FIMPs is depicted in Figure 3 with a DM mass $M_{\rm DM} = 100$ GeV and a thermal average annihilation cross-section $\langle \sigma v \rangle = 2 \times 10^{-21}$ GeV^{-2}. The dashed line ($x_{\rm fi}$) shows when the FIMPs freeze their number. The horizontal strip and the dot-dashed line are the same as before: the current relic density of DM and the temperature at which the BBN epoch starts, respectively. Again, the DM mass and thermal average annihilation cross-section parameters are excluded in the ΛCDM model because they overproduce the relic density.

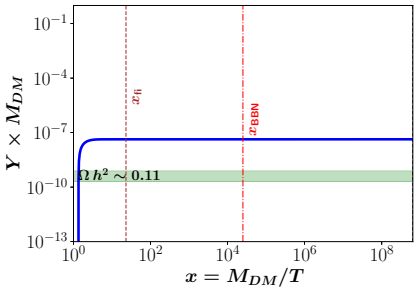

Figure 3. Yield of dark matter particles in standard cosmology with mass $M_{\rm DM} = 100$ GeV and thermal average annihilation cross-section $\langle \sigma v \rangle = 2 \times 10^{-27}$ GeV^{-2} established in the freeze in mechanism. These values of DM and $\langle \sigma v \rangle$ give rise to an overproduction of particles.

The numerical solution to Equations (13)–(17) provide the yield for the same values of previous parameters but with nonzero κ. In Figures 4 and 5, the yield for $\kappa = 10^{-35}$ and $\omega = 0$ is shown. Now, the DM relic agrees with the expected value today.

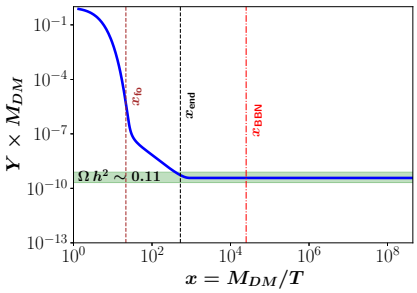

Figure 4. The yield of dark matter particles in the model of two scale-factors (FO mechanism). For the DM mass $M_{\rm DM} = 100$ GeV and thermal average annihilation cross-section $\langle \sigma v \rangle = 10^{-11}$ GeV^{-2}, the Poisson bracket deformation parameter is $\kappa = 10^{-35}$.

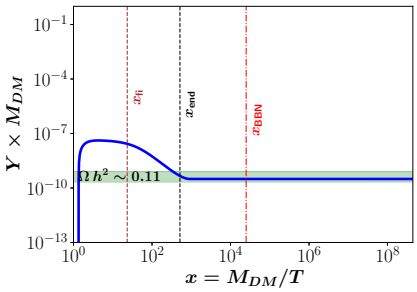

Figure 5. The yield of dark matter particles in the model of two scale-factors (FI mechanism). For the DM mass $M_{\rm DM} = 100$ GeV and thermal average annihilation cross-section $\langle \sigma v \rangle = 10^{-27}$ GeV^{-2}, the Poisson bracket deformation parameter is $\kappa = 10^{-35}$.

A few comments are in order here. In both figures, the vertical line $x_{\rm end}$ shows the temperature at which the energy of the patch b drained completely to a. For all calculations, we assumed a symmetric initial condition, namely that the initial energy densities in patches a and b are equal, where $\delta = 1$ (see Equation (12)), and we also assumed that the patch b was filled with nonrelativistic matter such that $\omega = 0$.

Parenthetically, in these calculations, we used $\rho_a + \rho_{\rm DM}$ at the RHS of Equation (14). Figure 6 shows the solutions obtained as before and the solution obtained when $\rho_a + \rho_{\rm DM} \approx \rho_a$ was assumed. No significant difference was observed; therefore, we can use this approximation for the case of axions, where numerical calculations are more involved.

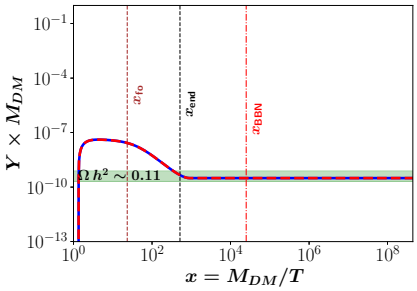

Figure 6. Comparison between considering the DM energy density in the Hubble parameter (blue line) and not considering it (red dashed line). As was noted, the contribution of DM energy density in the epoch of interest is too small compared with the radiation energy density, so in a certain way, it is possible to treat the equation as decoupled.

We also analyzed the case in which the energy content in patch b is radiation ($\omega = 1/3$), showing similar behavior. The parameter space in mass and the cross-section for different values of κ that reproduce the current DM relic density in the FI and FO cases have also been studied, showing that it is possible to enlarge the parameter space of DM.

To summarize, we can describe the DM process production as follows. Due to the interaction encoded in the Poisson bracket deformation (through a nonzero value of κ), the energy density in patch b decreases, and therefore, the radiation energy density in patch a increases. This might translate into a lowering of the WIMP and FIMP yield. Indeed, $Y = n_{\rm DM}/s$, and then for a set of parameters responsible for the DM overproduction in the standard cosmology, there will be an entropy increase due to the drain of energy from patch b to patch a so that the ratio Y has a chance to give the right value at the present time.

3. Axionic Dark Matter

3.1. Axionic Dark Matter

A different model for DM is the weakly interactive slim particles (WISPs). In this group, we find the axions [59]. These particles have a small mass, and thus they must be generated nonthermally [60] to avoid high momentum components. In what follows, we

will resume these mechanisms of dark matter (DM) production, focusing on the key aspects relevant to our proposal.

The most promising candidate is the so-called axion, the pseudo-Nambu–Goldstone boson arising after the Peccei–Quinn (PQ) $U(1)$ symmetry [59] is spontaneously broken, solving the strong CP problem. The scale at which the PQ symmetry breaks is related to the mass of the axion particle ($m_{\rm a}$) through

$$m_{\rm a}^2(T) = \frac{\chi(T)}{f_{\rm a}^2}, \tag{19}$$

where $\chi(T)$ is the topological susceptibility and $f_{\rm a}$ is the energy scale at which the symmetry breaks. The term $\chi(T)$ can be estimated, for example, from a QCD lattice simulation [61]. For numerical purposes we will use the results reported in [62]. It is worth mentioning that for analytical calculations, the axion mass is a constant for temperatures $T < T_{\rm QCD}$, while for $T > T_{\rm QCD}$, it depends on T^{-4} [63].

On the other hand, the axion's mass depends on f_a which, for our analysis, is a free parameter. However, instead of f_a, one uses the present axion mass; that is, $m_a \equiv \chi(0)/f_a$. We refer to this independent temperature as m_a, in contrast with $m_a(T)$, where the explicit temperature dependence is considered.

The axion Lagrangian density is given by

$$\mathcal{L} = \frac{1}{2}\partial_\mu\phi\partial^\mu\phi - m_a^2(T) f_a^2\left(1 - \cos\frac{\phi}{f_a}\right) \tag{20}$$

with ϕ being the Axion field.

We will analyze only the zero modes of the axion field, assuming that it is homogeneously distributed in the space (considering that the contribution to DM comes from this mode of oscillation [63–65]). The field equation, therefore, is

$$\ddot{\Theta} + 3\,H_a\,\dot{\Theta} + m_{\rm a}^2(T)\sin(\Theta) = 0, \tag{21}$$

with $\Theta = \phi(t)/f_{\rm a}$.

For a given initial condition θ (the initial misalignment angle), the axion starts to oscillate at a time $t_{\rm osc}$ until it reaches its true minimum $\Theta = 0$. The time $t_{\rm osc}$ corresponds to a temperature $T_{\rm osc}$, defined through the relation

$$\alpha H(T_{\rm osc}) = m_{\rm a}(T_{\rm osc}), \tag{22}$$

where α is a numerical factor in the range $[1, 3]$. In our case, we will use $\alpha = 3$, since it best fits the numerical results.

The energy tensor gives the axion energy density for a scalar field; in other words, we have

$$\begin{aligned} \rho_\phi &= \frac{1}{2}\dot{\phi}^2 + m_a^2(T)\, f_a^2\left(1 - \cos\frac{\phi}{f_a}\right), \\ &= f_a^2\left(\frac{1}{2}\dot{\Theta}^2 + m_a^2(T)(1 - \cos\theta)\right). \end{aligned} \tag{23}$$

From the numerical solution for Equation (21), and using the temperature-dependent mass in Equation (19), it is possible to calculate ρ_ϕ from the previous expression as a function of the free parameters θ and m_a.

It is also possible to proceed differently, which is suitable not only for numerical calculations but also for nonstandard cosmologies where entropy injection is present due to new matter fields. In our case, this entropy injection is caused by the presence of the other patch.

The approach above rests on the co-moving axion number N_ϕ being conserved; that is, $N_\phi(T_1) = N_\phi(T_2)$ for any two arbitrary temperatures T_1, T_2. With $N_\phi = n_\phi\, a^3$ and n_ϕ, the axion number is defined, for a nonrelativistic axion particle, through $\rho_\phi = n_\phi m_a(T)$.

By imposing the conservation at $T_1 = T_{\rm osc}$ and $T_2 = T_0$ (the current temperature of the universe), one finds

$$\rho_\phi(T_0) = \rho_\phi(T_{\rm osc}) \frac{m_a}{m_a(T_{\rm osc})} \frac{s(T_0)}{s(T_{\rm osc})}, \tag{24}$$

where the universe is assumed to expand adiabatically, and thus the scale factor a and the temperature are related according to $s(T) \propto a^{-3}$, with s being the entropy density. Therefore, $\left(a_{\rm osc}/a_{T_0}\right)^3 = s(T_0)/s(T_{\rm osc})$.

Finally, an analytic approximation for the energy density is obtained through $\rho_\phi(T_{\rm osc}) \simeq \frac{1}{2} m_{\rm a}(T_{\rm osc}) f_{\rm a}^2 \theta^2$, where θ is the initial misalignment angle which is a free parameter together with the non-dependent temperature mass of the axion m_a.

The fraction of energy produced by the axion field with respect to the critical density ρ_c is

$$\Omega_\phi = \frac{\rho_\phi(T_0)}{\rho_c}. \tag{25}$$

Let us discuss how this model of DM evolves in the model of the universe with two scale factors.

3.2. Axionic DM in the Bimetric Universe

In a universe with no DM component, the compatible values of κ are those that drain the energy density from one patch to another before the BBN starts (see [42]). When DM is considered, nonzero values of κ also affect the production of the DM's relic density due to the entropy injection. From now on, we will consider the energy content in patch a to be the radiation, and the energy content in b will be characterized by the barotropic index ω.

Since the main features of the axions are described in terms of the temperature of the universe, it is convenient to write all quantities of interest as a function of this temperature. For this, one must consider the entropy density, which satisfies the following in our model:

$$\dot{s} + 3Hs = 6\kappa M_{\rm Pl}^3 \frac{\dot{a}\dot{b}}{a^3}, \tag{26}$$

Considering that the main contribution to the entropy comes from photons, this equation tracks the temperature of the photons and, therefore, the energy density of the SM plasma. On the other hand, the SM entropy density can be written as

$$s = \frac{\rho_a + p_a}{T} = \frac{2\pi^2}{45} g_{\star s}(T) T^3, \tag{27}$$

with p_a being the pressure terms for the radiation content ($1/3 = p_a/\rho_a$) and $g_{\star s}(T)$ being the effective degrees of freedom for the entropy density.

The link between temperature and time is obtained from Equations (26) and (27). Indeed, from here, it is possible to find an expression for $\dot{T}$ for the photons, namely

$$\dot{T} = \left(1 + g'_{\star s}(T) \frac{T}{3 g_{\star s}(T)}\right)^{-1} \left(6\kappa M_{\rm Pl}^3 \frac{\dot{a}\dot{b}}{3 s(T) a^3} - T\frac{\dot{a}}{a}\right), \tag{28}$$

where $'$ denotes a derivative with respect to the temperature.

Assuming that the plasma in the SM content remains at internal equilibrium in the early universe, the energy density for the plasma can be related to the temperature through $\rho_a = \frac{\pi^2}{30} g_\star(T) T^4$ (radiation energy density), with $g_\star(T)$ being the relativistic degrees of freedom.

To summarize, the later relation for ρ_a, together with

$$\dot{\rho_b} + 3(\omega+1)\frac{\dot{b}}{b}\rho_b = -6\kappa M_{\rm Pl}^3 \frac{\dot{a}\dot{b}}{b^3}, \quad (29)$$

$$\ddot{\Theta} + 3\,H_a\,\dot{\Theta} + m_{\rm a}^2(T)\sin(\Theta) = 0, \quad (30)$$

$$\dot{a} = a\sqrt{\frac{\rho_a + \rho_{\rm DM}}{3M_{\rm Pl}^2}}, \quad (31)$$

$$\dot{b} = b\sqrt{\frac{\rho_b}{3M_{\rm Pl}^2}}. \quad (32)$$

describes the bi-metric universe with an axion DM. With the help of Equation (28), we can describe the evolution as a function of temperature instead of time. Note that the epoch we are interested in is characterized by the condition $\rho_a \gg \rho_{\rm DM}$, and then we can solve Equation (31) with just $\rho_a + \rho_{\rm DM} \approx \rho_a$. We have already shown that this is indeed a good approximation for the case of WIMPs and FIMPs. The same assumption will be used to calculate the axion evolution for axionic DM.

For the axion case, the energy density at the current time ($\rho_\phi(T_0)$, with T_0 as the current temperature) can be computed similar to the standard case. Still, we need to consider the injection of entropy due to the decay of the field in the b patch. Then, we have

$$\rho_\phi(T_0) = \rho_\phi(T_{\rm osc})\frac{m_{\rm a}}{m_{\rm a}(T_{\rm osc})}\frac{s(T_0)}{s(T_{\rm osc})} \times \frac{S_{\rm osc}}{S_{\rm end}}, \quad (33)$$

with $T_{\rm end}$ being the temperature at which the field in the patch a decays. The last factor ($S_{\rm osc}/S_{\rm end}$) is the dilution term [66] produced by the energy density increase in the a patch. This factor affects the DM production in the case of FIMPs and WIMPs.

We now discuss the effects of including a second scale factor b with a modified Poisson bracket structure in the production of axionic DM. In what follows, the ratio between the initial content of matter in b and a will be denoted as δ ($\delta = [\rho_b(T_{\rm ini})]/[\rho_a(T_{\rm ini})]$).

In Figure 7, we show the parameter space in the misalignment angle and the mass of the axion particle that reproduces the current DM relic density, varying the value of δ with fixed $\kappa = 10^{-34}$ and $\omega = 0$. The blue line corresponds to the case where patches a and b evolve independently ($\kappa = 0$) (i.e., the standard cosmological model). We observe that for lower values of δ, the region of parameters reproducing the actual value of the DM density was closer to the SM case. Note also that as δ diminishes, an intersection between the $\kappa \neq 0$ and the SM is present, which means that for a specific set of parameters, the bi-metric scenario with $\kappa \neq 0$ cannot be distinguished from the current DM relic density.

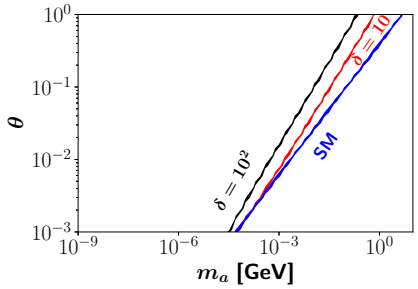

Figure 7. Parameter space that reproduces the DM relic density, varying δ for $\omega = 0$ and $\kappa = 10^{-34}$. The blue line represents the standard model case.

Figure 8 shows the parameter space in the misalignment angle and the mass of the axion particle that reproduces the current DM relic density, varying the value of ω with $\delta = 10^2$ and $\kappa = 10^{-34}$. It is noted that for higher values of ω, the region obtained was similar to the SM case. The case for $\omega = 2/5$ differed only for angles higher than $\theta \approx 10^{-2}$,

and thus for a large space of parameters, there was no difference between these two scenarios. Also, the slopes suggest a new point at which the regions intersect and cannot be distinguished from the cosmological scenario.

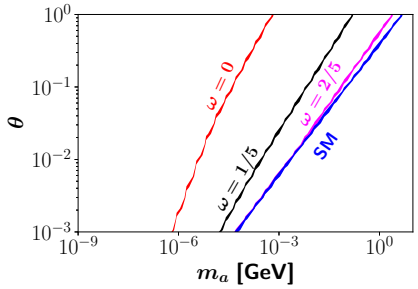

Figure 8. Parameter space that reproduces the DM relic density, varying ω for $\delta = 10^2$, $\kappa = 10^{-34}$ and $T_{\rm ini} = 10^3$. The blue line represents the standard model case.

In Figure 9, we present the parameter space in the misalignment angle and the mass of the axion particle that reproduces the current DM relic density, varying κ with $\delta = 10^2$ and $\omega = 0$. For higher values of κ, the region was closer to the SM case. This is contrary to the fact that when $\kappa = 0$, the SM case was restored. Again, the slopes in the region suggest a specific set of parameters that intersect.

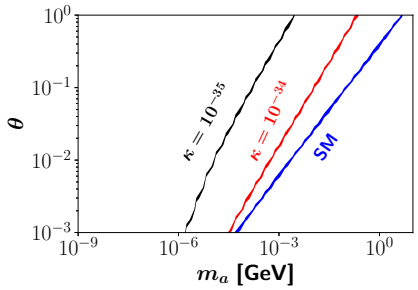

Figure 9. Parameter space that reproduced the DM relic density, varying κ for $\delta = 10^2$, $T_{\rm ini} = 10^2$ and $\omega = 0$. The blue line represents the standard model case.

Another interesting feature for the axion case is the temperature of oscillation ($T_{\rm osc}$), which did not change, varying the values of ω and δ or κ as shown in Figure 10. This means that the different regions shown in Figures 7–9 were only due to the dilution factor (entropy injection). There was no contribution for the time at which the axion started to oscillate.

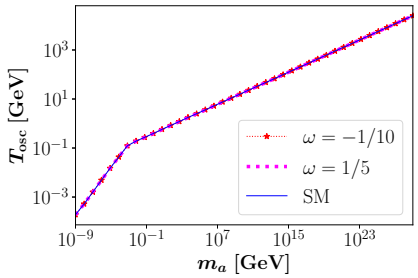

Figure 10. Temperature of oscillation for axion with different values of ω.

4. Discussion and Conclusions

This work presented the axionic DM evolution in a universe with two scale factors when considering a nonstandard Poisson bracket structure. The model was first considered in [20] and subsequent works [21,22], excluding any matter content to explore the structure of spacetime. However, in a more realistic scenario, it is natural to ask for the effects of

such modifications when ordinary matter and dark matter are present. The problem of incorporating standard matter into the model was addressed in a recent study [23].

It is then natural to ask if this nonstandard cosmology left imprints in DM production. The cases of WIMPs and FIMPs (for freeze out (FO) and freeze in (FI) mechanism production) were studied in [24]. The results for standard matter and the cases of DM production just mentioned were reviewed in Section 2 of the present work.

The present study is instead devoted to axion DM, a different candidate from DM. The main results of the present work are (1) the possibility of obtaining the current DM relic density, varying the fluid content of the *hidden* patch as well as the deformation parameter κ, which controls the entropy injection from b to a, (2) this mechanism creates a new way to generate a nonstandard cosmology but in a noninvasive mode (i.e., without an extra field in the early universe), and (3) the axion's temperature of oscillation does not change when varying the parameters of the cosmology under consideration. Let us comment on these results.

The entropy injection's behavior depended on the model's parameters, as expected. For example, by varying ω (the barotropic constant of matter in patch b), one can reach new regions in the misalignment angle and the axion mass. Lower values for ω are consistent with lower values for the axion mass; that is, nonrelativistic matter in b is compatible with smaller axion masses in a, compared with the relativistic matter in b, for a given value of κ. This allowed shift to the left region is shown in Figure 8.

On the other hand, lower values for κ and higher values for δ gave a behavior similar to the one described before, allowing us to reach lower masses for the axion. This behavior seems to contradict the result that, for $\kappa = 0$, we recovered the SM. However, one must remember that the system describing this model is highly nonlinear, and on the other hand, it is consistent with previous results for WIMPs and FIMPs, where lower values of κ are consistent with lower values of DM.

Let us point out the fact that a set of values for the extra parameters fitting the correct amount of DM existing is somehow expected. What is interesting, from our point of view, is that the model with two scale factors and the interaction via a deformed Poisson's bracket structure is still viable when DM is present. This was already tested for the case of WIMPs and FIMPs, but here, we also extended the result for the case of DM modeled as axion particles.

From the numerical analysis, on the other hand, we see that the values of ω, δ, and κ did not change the temperature of oscillation in the axion particle scenario, meaning that changes in the parameter space allowed it reproduce the current DM relic density coming from the entropy injection to patch a only. This is a new effect that is different from nonstandard cosmologies, which incorporates an extra Φ field in the early universe and produces changes in the oscillation temperature for axions [66]. Indeed, the new field Φ decays at a rate Γ related to the temperature at which this particle decays. In these scenarios, the parameter space for the DM relic density is also modified and even agrees with some of the parameter space shown here, but the model is completely different.

Finally, considering the results for the FO and FI mechanisms of DM production in [24] and the present results for axionic DM, we conclude that the two-scale factor scenario is a new nonstandard cosmological model. For instance, in an FO mechanism, values of $\langle \sigma v \rangle = 10^{-11}$ GeV^{-2}, $T_{\text{end}} = 0.1$ GeV, and $M_{DM} = 100$ GeV reproduce the DM relic density in nonstandard cosmologies [45] as well as in our model. For the FI mechanism, by choosing values of $\langle \sigma v \rangle = 10^{-22}$ GeV^{-2}, $T_{\text{end}} = 500$ GeV, and $M_{DM} = 100$ GeV, the current DM relic density can be reproduced [42], but not in the case of two-scale factors. For the axionic DM, we have already seen that the current DM relic was reproduced, but there was no change in the oscillation temperature.

To conclude, the present work shows the model's compatibility with a different type of DM candidate not considered in previous works. However, there are different scenarios where the model must be tested to verify its compatibility with the well-established results in cosmology. Indeed, the presence of a new parameter, κ, enlarges the possibility to fit the

model with the observations. But it is interesting to note that the order of magnitude of κ is not too different for the different models of DM considered here and in previous works.

Author Contributions: All authors contributed equally to this work. All authors have read and agreed to the published version of the manuscript.

Funding: This work was supported by Dicyt-USACH grants USA2155-Dicyt (CM) and POSTDOC_DICYT 042231MF_Postdoc, Vicerrectoría de Investigación, Desarrollo e Innovación.

Institutional Review Board Statement: Not applicable.

Informed Consent Statement: Not applicable.

Data Availability Statement: Not applicable.

Acknowledgments: We would like to thank Moira Venegas for helpful discussions.

Conflicts of Interest: The authors declare no conflict of interest.

References

1. Ashtekar, A.; Bianchi, E. A short review of loop quantum gravity. *Rept. Prog. Phys.* **2021**, *84*, 042001. [CrossRef]
2. Carlip, S.; Chiou, D.W.; Ni, W.T.; Woodard, R. Quantum gravity: A brief history of ideas and some prospects. In *One Hundred Years of General Relativity: From Genesis and Empirical Foundations to Gravitational Waves, Cosmology and Quantum Gravity*; World Scientific: Singapore, 2017; Volume 2, pp. 325–347. [CrossRef]
3. Oriti, D. *Approaches to Quantum Gravity: Toward a New Understanding of Space, Time and Matter*; Cambridge University Press: Cambridge, UK, 2009.
4. Kiefer, C. *Quantum Gravity*, 2nd ed.; Oxford University Press: New York, NY, USA, 2007.
5. Rovelli, C. Loop Quantum Gravity. *Living Rev. Relativ.* **1998**, *1*, 1. [CrossRef]
6. Addazi, A.; Alvarez-Muniz, J.; Batista, R.A.; Amelino-Camelia, G.; Antonelli, V.; Arzano, M.; Asorey, M.; Atteia, J.L.; Bahamonde, S.; Bajardi, F.; et al. Quantum gravity phenomenology at the dawn of the multi-messenger era—A review. *Prog. Part. Nucl. Phys.* **2022**, *125*, 103948. [CrossRef]
7. Rovelli, C. Considerations on Quantum Gravity Phenomenology. *Universe* **2021**, *7*, 439. [CrossRef]
8. Torri, M.D.C. Quantum Gravity Phenomenology Induced in the Propagation of UHECR, a Kinematical Solution in Finsler and Generalized Finsler Spacetime. *Galaxies* **2021**, *9*, 103. [CrossRef]
9. Hossenfelder, S. (Ed.) Experimental Search for Quantum Gravity. In Proceedings of the Giersch International Symposion 2016, Frankfurt, Germany, 19–23 September 2016; FIAS Interdisciplinary Science Series, 2018.
10. Amelino-Camelia, G. Quantum-Spacetime Phenomenology. *Living Rev. Relativ.* **2013**, *16*, 5. [CrossRef]
11. Brahma, S.; Ronco, M. Constraining the loop quantum gravity parameter space from phenomenology. *Phys. Lett. B* **2018**, *778*, 184–189. [CrossRef]
12. Dowker, F.; Henson, J.; Sorkin, R. Discreteness and the transmission of light from distant sources. *Phys. Rev. D* **2010**, *82*, 104048. [CrossRef]
13. Amelino-Camelia, G. Relativity in space-times with short distance structure governed by an observer independent (Planckian) length scale. *Int. J. Mod. Phys. D* **2002**, *11*, 35–60. [CrossRef]
14. Bojowald, M.; Morales-Tecotl, H.A.; Sahlmann, H. On loop quantum gravity phenomenology and the issue of Lorentz invariance. *Phys. Rev. D* **2005**, *71*, 084012. [CrossRef]
15. Carmona, J.M.; Cortes, J.L.; Gamboa, J.; Mendez, F. Noncommutativity in field space and Lorentz invariance violation. *Phys. Lett. B* **2003**, *565*, 222–228. [CrossRef]
16. Carmona, J.M.; Cortes, J.L.; Gamboa, J.; Mendez, F. Quantum theory of noncommutative fields. *JHEP* **2003**, *3*, 058. [CrossRef]
17. Carmona, J.M.; Cortes, J.L.; Das, A.K.; Gamboa, J.; Mendez, F. Matter-antimatter asymmetry without departure from thermal equilibrium. *Mod. Phys. Lett. A* **2006**, *21*, 883–892. [CrossRef]
18. Gamboa, J.; Loewe, M.; Mendez, F.; Rojas, J.C. The Landau problem and noncommutative quantum mechanics. *Mod. Phys. Lett. A* **2001**, *16*, 2075–2078. [CrossRef]
19. Horvathy, P.A. The Noncommutative Landau problem and the Peierls substitution. *Ann. Phys.* **2002**, *299*, 128–140. [CrossRef]
20. Falomir, H.; Gamboa, J.; Méndez, F.; Gondolo, P. Inflation without Inflaton: A Model for Dark Energy. *Phys. Rev. D* **2017**, *96*, 083534. [CrossRef]
21. Falomir, H.; Gamboa, J.; Gondolo, P.; Méndez, F. Magnetic Seed and Cosmology as Quantum Hall Effect. *Phys. Lett. B* **2018**, *785*, 399–402. [CrossRef]
22. Falomir, H.; Gamboa, J.; Mendez, F. A Noncommutative Model of Cosmology with Two Metrics. *Symmetry* **2020**, *12*, 435. [CrossRef]
23. Maldonado, C.; Mendez, F. Bimetric universe with matter. *Phys. Rev. D* **2021**, *103*, 123505. [CrossRef]
24. Maldonado, C.; Mendez, F. Dark Matter in a bi-metric universe. *Int. J. Mod. Phys. D* **2023**, *32*, 2350059. [CrossRef]
25. Cattaneo, A.S.; Indelicato, D. Formality and star products. *Lond. Math. Soc. Lect. Note Ser.* **2004**, *323*, 79–144. [CrossRef]

26. Kontsevich, M. Deformation quantization of Poisson manifolds. 1. *Lett. Math. Phys.* **2003**, *66*, 157–216. [CrossRef]
27. Fedosov, B.V. A simple geometrical construction of deformation quantization. *J. Differ. Geom.* **1994**, *40*, 213–238. [CrossRef]
28. Bayen, F.; Flato, M.; Fronsdal, C.; Lichnerowicz, A.; Sternheimer, D. Deformation Theory and Quantization. 1. Deformations of Symplectic Structures. *Ann. Phys.* **1978**, *111*, 61. [CrossRef]
29. Grasso, D.; Rubinstein, H.R. Magnetic fields in the early Universe. *Phys. Rep.* **2001**, *348*, 163–266. [CrossRef]
30. Kandus, A.; Kunze, K.E.; Tsagas, C.G. Primordial magnetogenesis. *Phys. Rep.* **2011**, *505*, 1–58. [CrossRef]
31. Nair, V.P.; Polychronakos, A.P. Quantum mechanics on the noncommutative plane and sphere. *Phys. Lett. B* **2001**, *505*, 267–274. [CrossRef]
32. Acatrinei, C. Path integral formulation of noncommutative quantum mechanics. *JHEP* **2001**, *9*, 007. [CrossRef]
33. Karabali, D.; Nair, V.P.; Polychronakos, A.P. Spectrum of Schrodinger field in a noncommutative magnetic monopole. *Nucl. Phys. B* **2002**, *627*, 565–579. [CrossRef]
34. Freidel, L.; Kowalski-Glikman, J.; Leigh, R.G.; Minic, D. Theory of metaparticles. *Phys. Rev. D* **2019**, *99*, 066011. [CrossRef]
35. Berglund, P.; Hübsch, T.; Minić, D. Dark Energy and String Theory. *Phys. Lett. B* **2019**, *798*, 134950. [CrossRef]
36. Berglund, P.; Hubsch, T.; Minic, D. Dark energy and quantum gravity. *Int. J. Mod. Phys. D* **2019**, *28*, 1944018. [CrossRef]
37. Berglund, P.; Hübsch, T.; Minic, D. String Theory, the Dark Sector and the Hierarchy Problem. *LHEP* **2021**, *2021*, 186. [CrossRef]
38. Freidel, L.; Kowalski-Glikman, J.; Leigh, R.G.; Minic, D. Quantum gravity phenomenology in the infrared. *Int. J. Mod. Phys. D* **2021**, *30*, 2141002. [CrossRef]
39. Particle Data Group; Zyla, P.; Barnett, R.M.; Beringer, J.; Dahl, O.; Dwyer, D.A.; Groom, D.E.; Lin, C.J.; Lugovsky, K.S.; Pianori, E.; et al. Review of Particle Physics. *PTEP* **2020**, *2020*, 083C01. [CrossRef]
40. Giudice, G.F.; Kolb, E.W.; Riotto, A. Largest temperature of the radiation era and its cosmological implications. *Phys. Rev. D* **2001**, *64*, 023508. [CrossRef]
41. Visinelli, L. (Non-)Thermal Production of WIMPs during Kination. *Symmetry* **2018**, *10*, 546. [CrossRef]
42. Maldonado, C.; Unwin, J. Establishing the dark matter relic density in an era of particle decays. *JCAP* **2019**, *6*, 37. [CrossRef]
43. Bernal, N.; Elahi, F.; Maldonado, C.; Unwin, J. Ultraviolet Freeze-in and Non-Standard Cosmologies. *JCAP* **2019**, *11*, 26. [CrossRef]
44. Bernal, N.; Ghoshal, A.; Hajkarimc, F.; Lambiase, G. Primordial gravitational wave signals in modified cosmologies. *JCAP* **2020**, *11*, 051. [CrossRef]
45. Arias, P.; Bernal, N.; Herrera, A.; Maldonado, C. Reconstructing non-standard cosmologies with dark matter. *JCAP* **2019**, *10*, 47. [CrossRef]
46. Chung, D.J.H.; Kolb, E.W.; Riotto, A. Production of massive particles during reheating. *Phys. Rev. D* **1999**, *60*, 063504. [CrossRef]
47. Kolb, E.W.; Notari, A.; Riotto, A. Reheating stage after inflation. *Phys. Rev. D* **2003**, *68*, 123505. [CrossRef]
48. Bertone, G.; Hooper, D.; Silk, J. Particle dark matter: Evidence, candidates and constraints. *Phys. Rept.* **2005**, *405*, 279–390. [CrossRef]
49. Arcadi, G.; Dutra, M.; Ghosh, P.; Lindner, M.; Mambrini, Y.; Pierre, M.; Profumo, S.; Queiroz, F.S. The waning of the WIMP? A review of models, searches, and constraints. *Eur. Phys. J.* **2018**, *C78*, 203. [CrossRef]
50. Lin, T. Dark matter models and direct detection. *PoS* **2019**, *333*, 009. [CrossRef]
51. Hooper, D. TASI Lectures on Indirect Searches For Dark Matter. *PoS* **2019**, *TASI2018*, 010.
52. Kolb, E.W.; Turner, M.S. *The Early Universe*; CRC Press: Boca Raton, FL, USA, 1990; Volume 69.
53. Hall, L.J.; Jedamzik, K.; March-Russell, J.; West, S.M. Freeze-In Production of FIMP Dark Matter. *JHEP* **2010**, *1003*, 080. [CrossRef]
54. Chu, X.; Hambye, T.; Tytgat, M.H.G. The Four Basic Ways of Creating Dark Matter Through a Portal. *JCAP* **2012**, *1205*, 034. [CrossRef]
55. Bernal, N.; Heikinheimo, M.; Tenkanen, T.; Tuominen, K.; Vaskonen, V. The dawn of FIMP Dark Matter: A review of models and constraints. *Int. J. Mod. Phys. A* **2017**, *32*, 1730023. [CrossRef]
56. McDonald, J. Thermally generated gauge singlet scalars as selfinteracting dark matter. *Phys. Rev. Lett.* **2002**, *88*, 091304. [CrossRef]
57. Choi, K.Y.; Roszkowski, L. E-WIMPs. *AIP Conf. Proc.* **2006**, *805*, 30–36. [CrossRef]
58. Kusenko, A. Sterile neutrinos, dark matter, and the pulsar velocities in models with a Higgs singlet. *Phys. Rev. Lett.* **2006**, *97*, 241301. [CrossRef] [PubMed]
59. Peccei, R.D.; Quinn, H.R. CP Conservation in the Presence of Instantons. *Phys. Rev. Lett.* **1977**, *38*, 1440. [CrossRef]
60. Nelson, A.E.; Scholtz, J. Dark Light, Dark Matter and the Misalignment Mechanism. *Phys. Rev. D* **2011**, *84*, 103501. [CrossRef]
61. Gorghetto, M.; Villadoro, G. Topological Susceptibility and QCD Axion Mass: QED and NNLO corrections. *JHEP* **2019**, *3*, 033. [CrossRef]
62. Borsányi, S.; Fodor, Z.; Guenther, J.; Kampert, K.H.; Katz, S.D.; Kawanai, T.; Kovacs, T.G.; Mages, S.W.; Pasztor, A.; Pittler, F.; et al. Calculation of the axion mass based on high-temperature lattice quantum chromodynamics. *Nature* **2016**, *539*, 69. [CrossRef]
63. Hertzberg, M.; Tegmark, M.; Wilczek, F. Axion Cosmology and the Energy Scale of Inflation. *Phys. Rev. D* **2008**, *78*, 083507. [CrossRef]
64. Harani, D.; Sikivie, P. On the evolution of global strings in the early universe. *Phys. Lett. B* **1987**, *195*, 361.[CrossRef]

65. Ramberg, N.; Visinelli, L. Probing the early Universe with ax- ion physics and gravitational waves. *Phys. Rev. D* **2019**, *99*, 123513. [CrossRef]
66. Arias, P.; Bernal, N.; Karamitros, D.; Maldonado, C.; Roszkowski, L.; Venegas, M. New opportunities for axion dark matter searches in nonstandard cosmological models. *JCAP* **2021**, *11*, 003. [CrossRef]